scientific reports

Check for updates

OPEN

Doping effects of indium and copper on ferromagnetism in *N*-type magnetic semiconductor $Ba(Zn,Co)_2As_2$

Xueqin Zhao[1], Jinou Dong[1], Lingfeng Xie[1], Qiaolin Yang[1], Xun Pan[1], Haoyuan Tang[1], Zhicheng Xu[1], Guoxiang Zhi[1], Yilun Gu[1], Licheng Fu[1]✉ & Fanlong Ning[1,2,3,4]✉

We report the manipulation of ferromagnetism in *n*-type magnetic semiconductor $Ba(Zn,Co)_2As_2$ through carriers' doping. Doping In or Cu into Zn-sites introduces additional *n*-type or *p*-type carriers, respectively. Focusing on $Ba(Zn_{0.97}Co_{0.03})_2As_2$ which has a $T_C \sim 31$ K, In doping introduces additional *n*-type carriers and 2% In doping drastically improves the ferromagnetic transition temperature by 16% to 36 K. In contrast, 1.5% Cu doping suppresses T_C by 52% to 15 K; 3% Cu doping turns the dominant carrier to *p*-type, and eventually transforms the ferromagnetic ordering into a paramagnetic state. Our experimental results unequivocally demonstrate that the magnetic ordering in $Ba(Zn,Co)_2As_2$ is carriers' mediated ferromagnetism, and its ground states can be manipulated by carriers.

Magnetic semoconductors (MSs), which show both properties of semiconductors and ferromagnets, are the main sub-field of spintronics. In past few decades, a variety of thin film and bulk form MSs have been discovered[1–6]. Based on these materials, many interesting phenomena were reported and several spintronic devices were fabricated[1–8]. The most famous MSs are (Ga,Mn)As thin films that are synthesized through low temperature Molecular Beam Epitaxy (LT-MBE) method[9,10]. In (Ga,Mn)As, Mn/Ga substitution induces both spins and holes simultaneously and turns the system into ferromagnetic state when the doping level of Mn exceeds $\sim$ 1%. (Ga,Mn)As behaves as a *p*-type MS with carrier concentrations of 10^{20}-10^{21}/cm^{-3}. Theoretical studies show that the spin-spin exchange interactions in (Ga,Mn)As are mediated by holes and can be enhanced with increasing carrier concentrations[11,12]. As of today, the highest ferromagnetic transition temperature T_C observed in (Ga,Mn)As is $\sim$ 200 K, with the doping level of Mn up to $\sim$ 12%[13]. In 2012, Tanaka et al. reported the *n*-type MS (In,Fe)As thin films, in which the spins are induced by Fe while carriers are induced by native defects and non-magnetic donors. That is, the carrier concentration can be regulated while fixing the spin concentration. Their results show that the Curie temperature in (In,Fe)As increases as carrier concentration increases, indicating that the ferromagnetism in (In,Fe)As is mediated by carriers[4,14].

In recent years, many series of bulk form MSs with decoupled spins and carriers doping have been reported, e.g. 111-type Li(Zn,Mn)As[15] and Li(Zn,Mn)P[16], 1111-type (La,Ba)(Zn,Mn)AsO[17] and 122-type (Ba,K)$(Zn,Mn)_2As_2$[18,19]. Through manipulating the spins' and carriers' concentrations separately, the individual dependencies of ferromagnetic ordering on spins or carriers have been carefully studied[18,20–22]. It has been demonstrated that the exchange interactions between spins are mediated by carriers in these bulk form MSs. To achieve the highest Curie temperature, both concentrations of spins and carriers have to be optimized. The highest T_C observed experimentally in bulk form MSs has been achieved as high as 230 K in $(Ba,K)(Zn,Mn)_2As_2$[19].

The dominant carriers of above mentioned bulk form MSs are holes, that is, they are *p*-type MSs. In 2019, our group has reported the successful fabrication of a new bulk form *n*-type MS $Ba(Zn,Co)_2As_2$[23]. The highest T_C reaches $\sim$ 45 K when the doping level of Co is up to 0.04, and muon spin relaxation (μSR) measurements have confirmed that the ferromagnetic ordering in $Ba(Zn,Co)_2As_2$ is homogeneous and intrinsic. In 2021, Fu et al.[24] have investigated the manipulation of ferromagnetic ordering in $Ba(Zn,Co)_2As_2$ system by negative and positive chemical pressure introduced by isovalent Sb/As and Sr/Ba substitutions, respectively, and found that T_C increased significantly in Sr-doped $Ba(Zn,Co)_2As_2$. In order to investigate the origin of *n*-type carriers

[1]School of Physics, Zhejiang University, Hangzhou 310027, China. [2]State Key Laboratory of Silicon and Advanced Semiconductor Materials, Zhejiang University, Hangzhou 310027, China. [3]Collaborative Innovation Center of Advanced Microstructures, Nanjing University, Nanjing 210093, China. [4]Science and Technology Innovation Center, Chifeng High-Tech Industrial Development Zone, Chifeng 025250, China. ✉email: lcfu@zju.edu.cn; ningfl@zju.edu.cn

in $Ba(Zn,Co)_2As_2$, Zhi et al[25]. performed systematic first-principles calculations on the electronic structure of $Ba(Zn,Co)_2As_2$. It has been found that carriers in $Ba(Zn,Co)_2As_2$ emerge when two (or more) Co atoms substitute for Zn atoms at adjacent lattice sites, and the density is predominantly contributed by As-4*p* orbitals, with subsidiary contributions from the Co-3*d* orbitals. In addition, Zhi et al. calculated the formation energies (E_f) of Co/Zn substitution and alternative defects, such as Co/Ba substitution and As vacancies[25]. The calculated results have revealed that comparing with E_f for Co/Ba substitution ($E_f \sim 5.1$ eV) and an As vacancy ($E_f \sim 1.9$ eV), E_f for Co/Zn substitution is significantly lower ($E_f \sim$ -0.4 eV). This further confirms that *n*-type carriers arise from hetero-valent Co/Zn substitution, and not arising from defects. While different to other bulk form *p*-type MSs, Co doping $Ba(Zn,Co)_2As_2$ introduces both spins and electron carriers (confirmed by Hall effect and Seebeck effect measurements[23]) simultaneously, which makes it difficult to investigate the individual influence of carriers and spins on the formation of ferromagnetism. Therefore, how the ferromagnetism in $Ba(Zn,Co)_2As_2$ is mediated by carriers has yet to be investigated.

In this paper, we report the effect of carriers doping on the ferromagnetism in *n*-type MS $Ba(Zn,Co)_2As_2$. Focusing on $Ba(Zn_{0.97}Co_{0.03})_2As_2$ which has a $T_C \sim 31$ K, additional *n*-type or *p*-type carriers have been introduced through In/Zn or Cu/Zn substitutions, respectively. The X-ray diffraction results show that all In-doped and Cu-doped samples maintain the high-temperature tetragonal structure. Hall effect measurements confirm that In doping introduces additional *n*-type carriers, and Cu doping introduces additional *p*-type carriers. DC magnetization measurements indicate that 2% In/Zn substitution significantly improves T_C of $Ba(Zn_{0.97}Co_{0.03})_2As_2$ by 16% to 36 K. On the other hand, 1.5% Cu doping obviously suppresses T_C by 52% to 15 K, and eventually transforms the ferromagnetic ordering into a paramagnetic state with 3% Cu doping. Our experimental results show that the ferromagnetism in *n*-type MS $Ba(Zn,Co)_2As_2$ can be manipulated by additional carriers through non-equivalent chemical doping, not only the concentrations but also the type of carrier.

Results and discussion

X-ray diffraction

Depending on the synthesis condition, $BaZn_2As_2$ exhibits two different crystal structures, the low-temperature orthorhombic phase α -$BaZn_2As_2$ (space group Pnma, metal)[26] and the high-temperature tetragonal phase β-$BaZn_2As_2$ (space group I4/mmm, semiconductor with a bandgap $\sim$ 0.2 eV)[27,28]. We should note that all $BaZn_2As_2$-based MSs can be realized only in the tetragonal phase β-$BaZn_2As_2$, as reported previously[18,23]. We conducted X-ray diffraction to determine the crystal structure, and show polycrystalline X-ray diffraction patterns of In-doped $Ba(Zn_{0.97-x}Co_{0.03}In_x)_2As_2$ (x = 0, 0.01, 0.02, 0.03 and 0.04) and Cu-doped $Ba(Zn_{0.97-x}Co_{0.03}Cu_x)_2As_2$ (x = 0.015 and 0.03) samples in Fig. 1a. With In or Cu doping, the peaks just shift slightly and no new peaks are found, which demonstrates that neither In/Zn nor Cu/Zn substitution breaks the tetragonal crystal structure, as shown in Fig. 1b. We also carried out the Rietveld refinements for the X-ray diffraction data of all samples with tetragonal β-$BaZn_2As_2$ phase using an open-source package GSAS-II[29], and show the Rietveld refinement result of $Ba(Zn_{0.95}Co_{0.03}In_{0.02})_2As_2$ in Fig. 1c as an example. The resultant weighted reliable factor R_{wp} is $\sim$ 6.5%, indicating the good fitting. The lattice parameters *a* and *c* can be obtained from the refinements. In Fig. 1d, we show the lattice parameters of all the samples. The obtained lattice constants a = 4.1221 Å and c = 13.5709 Å of the starting compound $Ba(Zn_{0.97}Co_{0.03})_2As_2$ agree well with those reported in previous work[23]. For In-doped samples, both the lattice constants *a* and *c* increase monotonically as the doping level x increases. For Cu-doped samples, with the increasing of Cu doping levels, the lattice constant *a* increases, while *c* decreases. We should note that the overall change of lattice parameters is quite small. The unit cell volume just increases $\sim$ 0.3% at the highest In doping level and decreases $\sim$ 0.4% at the highest Cu doping level.

Transport and Hall effect

The temperature-dependent resistivity of both In-doped and Cu-doped $Ba(Zn_{0.97}Co_{0.03})_2As_2$ samples are shown in Fig. 2a. For all In-doped samples, the resistivity increases with the decreasing of temperature, indicating that the samples retain semiconducting behavior. The magnitude of resistivity for In-doped samples decreases significantly with the increasing of In doping level, which agrees with our expectation that In/Zn substitution will induce more carriers. While for Cu-doped samples, the resistivity decreases with temperature decreasing, indicating that the samples change from semiconductor to metal, and the magnitude is much lower than that of In-doped samples in low temperature region. To examine the type and the concentrations of carriers for both In-doped and Cu-doped samples, we carried out the Hall effect measurements, and show the results in Fig. 2b–d. For the starting compound $Ba(Zn_{0.97}Co_{0.03})_2As_2$, due to the poor signal-to-noise ratio in low temperature region, we only show the experimental result measured at 300 K. The negative slope indicates that the dominant carriers are electrons, with a concentration $\sim 6\times 10^{17}/cm^{-3}$. As shown in Fig. 2c, for Cu-doped sample, the slopes of Hall resistivity curves at different temperature are all positive, indicating that the dominant carriers already change from electrons to holes. The carrier concentration obtained from the slope at different temperatures is quite close, $\sim 3\times 10^{20}/cm^{-3}$,which agrees with the metallic behavior observed in the resistivity measurement. While for In-doped samples, as shown in Fig. 2d, the *n*-type carriers are confirmed by Hall resistivity results as the slope is negative. The carrier concentration also increases with temperature increasing, which is also consistent with the semiconducting behavior. The carrier concentration at 300 K is $\sim 2\times 10^{19}/cm^{-3}$, two orders higher than that of $Ba(Zn_{0.97}Co_{0.03})_2As_2$. According to the formula $\sigma = ne\mu$, where σ, n, e and μ represent electrical conductivity, carrier concentration, elementary charge and carrier mobility, respectively, we calculate the carrier mobility of $Ba(Zn_{0.97}Co_{0.03})_2As_2$ and $Ba(Zn_{0.93}Co_{0.03}In_{0.04})_2As_2$ at 300 K that are 3.6 $cm^2/V\cdot s$ and 8.5 $cm^2/V\cdot s$, respectively. The improvement in carrier mobility is likely attributed to increased carrier concentration, which enhances the screening effect, thereby weakening the carrier scattering[30]. Our results demonstrate that In/Zn substitution induces more *n*-type carriers and conserves the semiconducting behavior

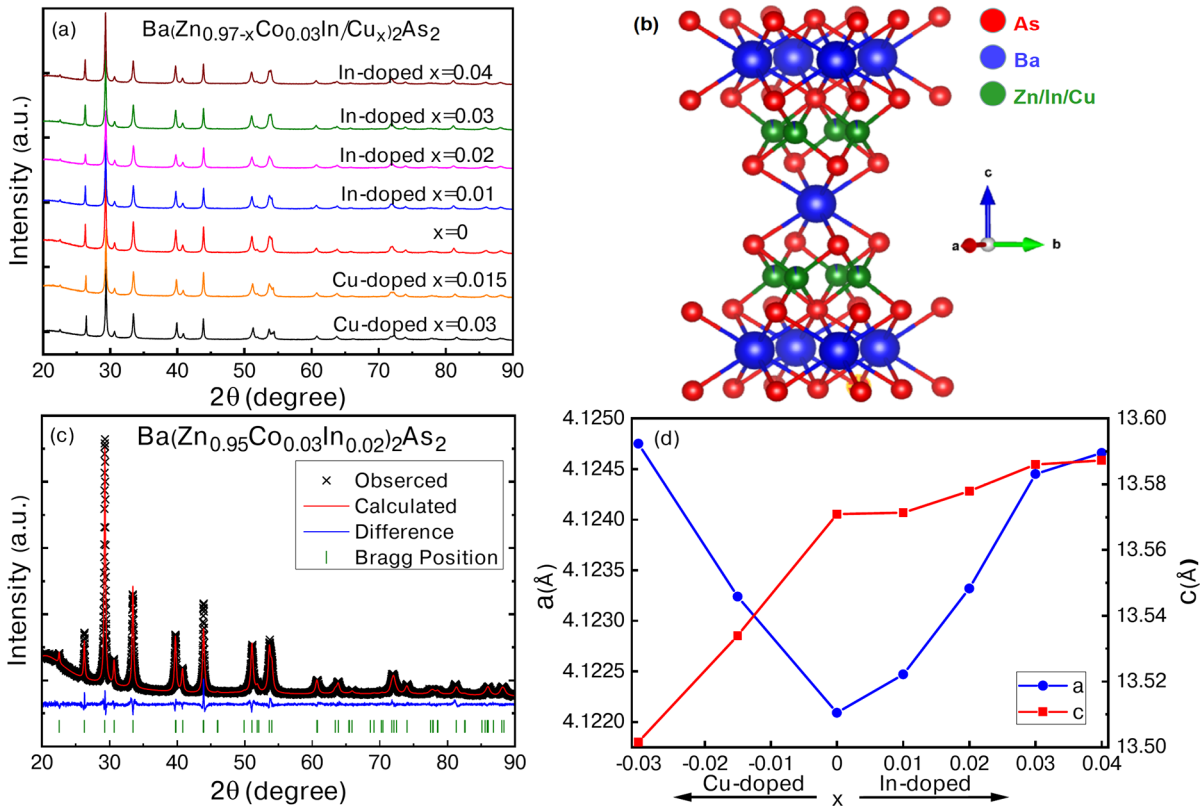

Fig. 1. (**a**) The X-ray diffraction patterns for polycrystalline In-doped $Ba(Zn_{0.97-x}Co_{0.03}In_x)_2As_2$ ($x = 0.01$, 0.02, 0.03 and 0.04) and Cu-doped $Ba(Zn_{0.97-x}Co_{0.03}Cu_x)_2As_2$ ($x = 0.015$ and 0.03). (**b**) The crystal structure of $BaZn_2As_2$ with high-temperature tetragonal phase. (**c**) The Rietveld refinement of $Ba(Zn_{0.95}Co_{0.03}In_{0.02})_2As_2$. (**d**) The lattice parameters *a* and *c* obtained from the Rietveld refinements for both In-doped and Cu-doped samples.

in $Ba(Zn_{0.97-x}Co_{0.03}In_x)_2As_2$, while Cu/Zn substitution induces *p*-type carriers and turns the semiconductor to metal in $Ba(Zn_{0.97-x}Co_{0.03}Cu_x)_2As_2$.

Magnetic properties

In Fig. 3a, we show the temperature-dependent DC magnetization for both In-doped and Cu-doped samples measured in field cooling (FC) modes under an applied external field of 100 Oe. Above 60 K, no magnetic instability can be observed for all samples. At lower temperatures, sharp increase appears, indicating the onset of ferromagnetic ordering. In the inset of Fig. 3a, we can see clearly the evolution of ferromagnetic transition with the doping level *x*. Compared with the starting compound $Ba(Zn_{0.97}Co_{0.03})_2As_2$, the transition temperature shifts to higher temperature region with In doping level increasing from 0 to 0.02, and then remain almost unchanged. In contrast, the transition temperature quickly shifts to lower temperature region with 1.5% Cu doping. When Cu-doping level reaches 0.03, the ferromagnetic transition is completely suppressed; The magnetization at 2 K is only $0.0043\mu_B$/Co, which is two orders of magnitude smaller than that of the starting compound $Ba(Zn_{0.97}Co_{0.03})_2As_2$. In Fig. 3(b) and (c), we show the iso-thermal magnetization curves $M(H)$ for both In-doped and Cu-doped samples measured at 2 K. Clear hysteresis loops can be observed in Cu-doped sample with doping level $x = 0.015$ and all the In-doped samples, which demonstrates the ferromagnetic ordering state. The coercive field of these samples are quite small, ~ 10 Oe, comparable to that of the starting compound $Ba(Zn_{0.97}Co_{0.03})_2As_2$. Such a small coercive field is good for spin manipulation. For the sample with 3% Cu doping, no hysteresis loop can be observed, which indicates that the ground state has been transformed into a paramagnetic state. We fit the paramagnetic part of the T-dependent magnetization data with a modified Curie–Weiss formula, $(\chi - \chi_0)^{-1} = (T - \theta)/c$, χ_0, C and θ represent the temperature-independent term, the Curie constant, and the Weiss temperature, respectively. From the fitting results, we can obtain the Weiss temperature θ and the effective momentum μ_{eff} by using the formula $C = N\mu_0\mu_{eff}^2/3k_B$. The effective momentum μ_{eff} is $\sim$ 1.4-1.7 μ_B/Co, which is close to the expected value of 1.7 μ_B/Co for $S = 1/2$[23]. Based on the experimental observation of the magnetization of 0.2-0.3 μ_B/Co in $M(T)$ curves at 2 K, we think that antiferromagnetic interactions exist between certain Co ions in the system. Specifically, the competition between ferromagnetic and antiferromagnetic interactions results in the reduced magnetization. The evolution of the Weiss temperature θ can also be seen clearly through the linear fitting of the reverse of $(\chi - \chi_0)$ versus temperature in the high temperature region, which is plotted in Fig. 4a and b. θ can be read from the the intersections of the linear fitting

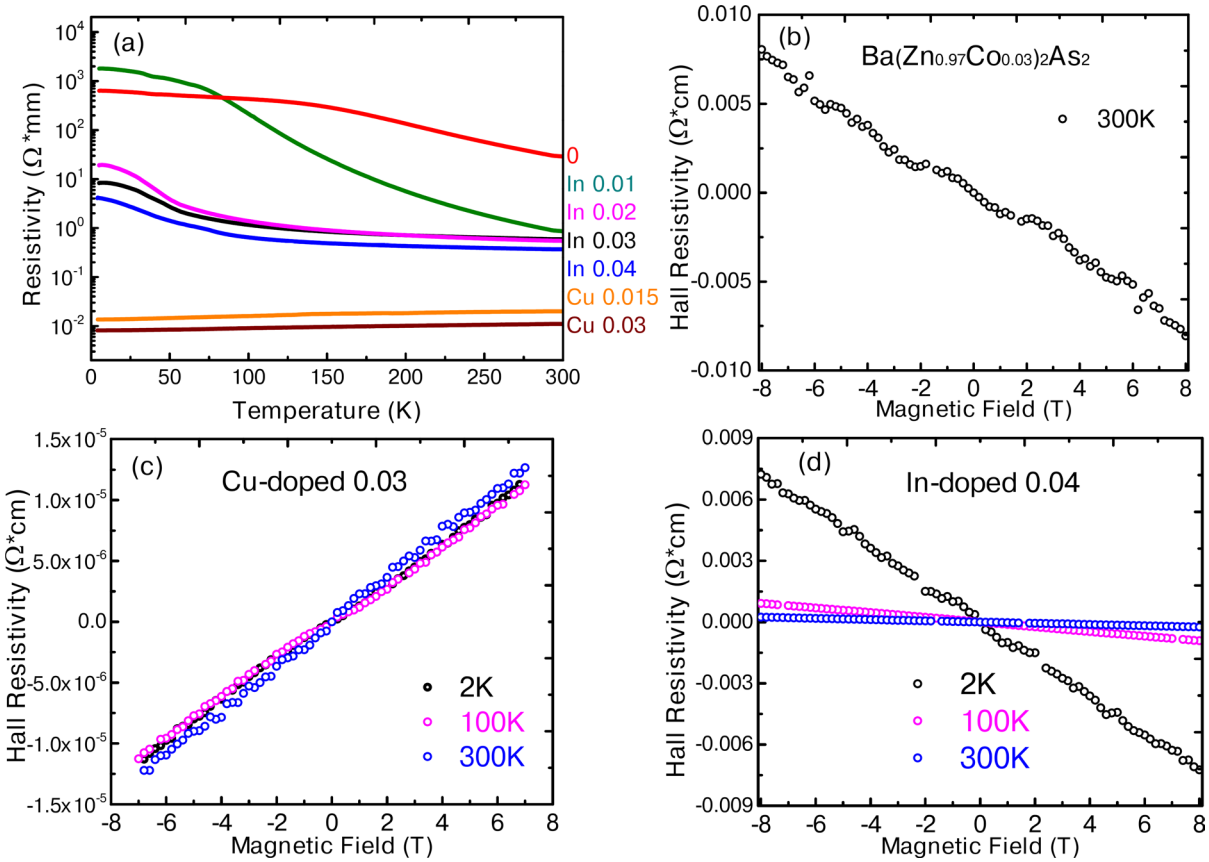

Fig. 2. (**a**) Temperature-dependent resistivity of In-doped and Cu-doped $Ba(Zn_{0.97}Co_{0.03})_2As_2$ samples. (**b**–**d**) Hall resistivity of (**b**) $Ba(Zn_{0.97}Co_{0.03})_2As_2$, (**c**) $Ba(Zn_{0.94}Co_{0.03}Cu_{0.03})_2As_2$ and (**d**) $Ba(Zn_{0.93}Co_{0.03}In_{0.04})_2As_2$.

lines and x axis. In Fig. 4c and d, we show the $dM(T)/dT$ versus temperature curves for all the samples, and the Curie temperature T_C were defined as the temperatures where $dM(T)/dT$ versus T curve shows a minimum.

We tabulate the Curie temperature T_C, the Weiss temperature θ, the effective moment μ_{eff} and M_{2K} (the M value measured at T = 2 K and H = 100 Oe in FC condition) in Table 1. We can see that both T_C and θ reach a maximum at x = 0.02 for In-doped samples, and then T_C remain unchanged while θ slightly rollback with more In doping. For $x \geq 0.02$, the variation of both T_C and θ is quite small (less than 2 K). In some cases, over-doping carriers may suppress the ferromagnetic ordering, which has been experimentally verified in some bulk form MSs like Li(Zn,Mn)P[22] and Li(Cd,Mn)P[31]. The carrier-mediated ferromagnetism can be described by the RKKY-like exchange interaction as $J \sim \cos(2k_F r)/r^3$, where k_F is the radius of Fermi surface and r is the distance between localized spins. Extra carriers will modify the Fermi surface, thus affects the value of J, and then the ferromagnetic ordering. While for Cu-doped samples, both T_C and θ decrease rapidly with the increasing of Cu doping level, and reach nearly 0 for x = 0.03, indicating the disappearence of ferromagnetism. Combining the results of In/Zn and Cu/Zn substitutions in $Ba(Zn_{0.97}Co_{0.03})_2As_2$ together, we can readily find that appropriate In/Zn substitution enhances the Curie temperature of ferromagnetic ordering, while Cu/Zn substitution suppresses the ferromagnetic ordering.

Summary

In previous report, the ferromagnetic ordering in $Ba(Zn,Co)_2As_2$ can be manipulated by chemical pressure[24], and the isovalent Sb/As and Sr/Ba substitutions don't induce extra carriers directly. The experimental results have revealed that Sb/As substitution induces negative chemical pressure through expanding lattice, which results in the decreasing of T_C; While Sr/Ba substitution induces positive chemical pressure through compressing lattice, which results in the increasing of T_C. In current work, In/Zn substitution induces extra n-type carriers and Cu/Zn substitution induces extra p-type carriers, but the variation of unit cell volume is very small, which is only $\sim$ 0.3% for the highest In doping level x = 0.04 and $\sim$ 0.4% for the highest Cu doping level x = 0.03; That means doping In or Cu introduces very small chemical pressure. The Curie temperature T_C for $Ba(Zn_{0.97}Co_{0.03})_2As_2$ is defined as 31 K by reading from the minimum of $dM(T)/dT$ versus T curves. We can see that 2% In/Zn substitution increases T_C by 16% from 31 K to 36 K. But for the highest Cu doping level x = 0.03, the ferromagnetic ordering has even been completely suppressed and transformed into a paramagnetic state, which is much more significant than the effect on T_C by negative chemical pressure induced by Sb/As substitutions.

To summerize, in this work, based on n-type MS $Ba(Zn_{0.97}Co_{0.03})_2As_2$, In/Zn and Cu/Zn substitution have been designed, and the doping effects have been investigated. Our X-ray diffraction results have demonstrated

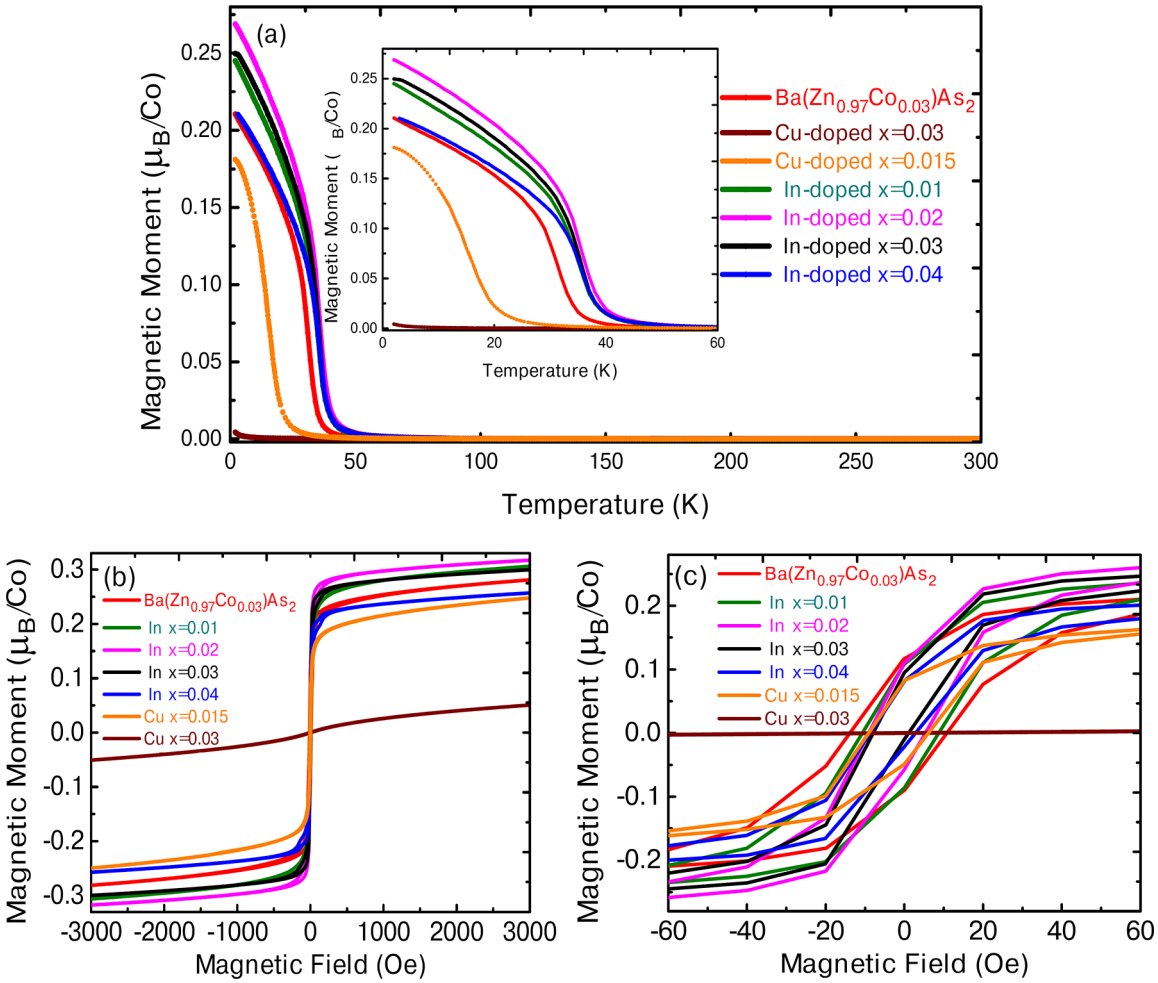

Fig. 3. (**a**) Temperature dependent DC magnetization for In-doped and Cu-doped samples in FC mode with an applied external field of 100 Oe. Inset shows the enlarged curves of 2 K to 60 K region. (**b**) The isothermal magnetization curves $M(H)$ measured at 2 K for both In-doped and Cu-doped samples. (**c**) Partial enlarged $M(H)$ curves with external field from − 60 Oe to 60 Oe.

that both In and Cu dopings will not affect the tetragonal crystal structure, and the lattice parameters do not change much at the highest doping levels of In and Cu. Through the Hall effect measurements, we find that In doping introduces additional electron carriers into the system, and improves the Curie temperature from 31 K to 36 K at the doping level $x = 0.02$, that is, 2% In doping into $Ba(Zn_{0.97}Co_{0.03})_2As_2$ improves T_C by 16%. With more In doping, the magnitude of resistivity is decreasing, while the Curie temperature T_C does not linearly increase, and the ferromagnetic ordering display RKKY-like exchange interactions. On the other hand, Cu doping induces extra hole carriers, which eventually suppresses the ferromagnetic ordering in $Ba(Zn_{0.97}Co_{0.03})_2As_2$ at the doping level of 3% Cu. Our work experimentally demonstrated that the mechanism of the ferromagnetic long range ordering in $Ba(Zn_{1-x-y}Co_xIn_y)_2As_2$ are consistent with the general carrier mediated ferromagnetism picture that has been proposed for MSs[3,8], and the ground state can be effectively manipulated by carriers' densities. This finding is helpful to understand the general mechanism responsible for the long range ferromagnetic ordering in all magnetic semiconductors.

Methods

Material synthesis

In-doped $Ba(Zn_{0.97-x}Co_{0.03}In_x)_2As_2$ and Cu-doped $Ba(Zn_{0.97-x}Co_{0.03}Cu_x)_2As_2$ polycrystalline samples were synthesized through conventional solid-state reaction method, similarly to that of $Ba(Zn,Co)_2As_2$[23]. Starting materials Ba pieces, In, Zn, Co, As, Cu powders were well mixed according to the elementary ratio and transferred to alumina crucibles and finally sealed in evacuated silica tubes. The mixture was heated at 1150 °C for 25 h followed by cooling to room temperature. The obtained products were then grounded, pressed into pellets with 8 mm in diameter, placed in aluminum crucibles, then sealed in evacuated silica tubes and reheated at 1150 °C for another 25 h for sufficient reaction. After heating, the samples were quickly cooled to room temperature through quenching in the water to stabilize the high-temperature phase, tetragonal β-$BaZn_2As_2$[32].

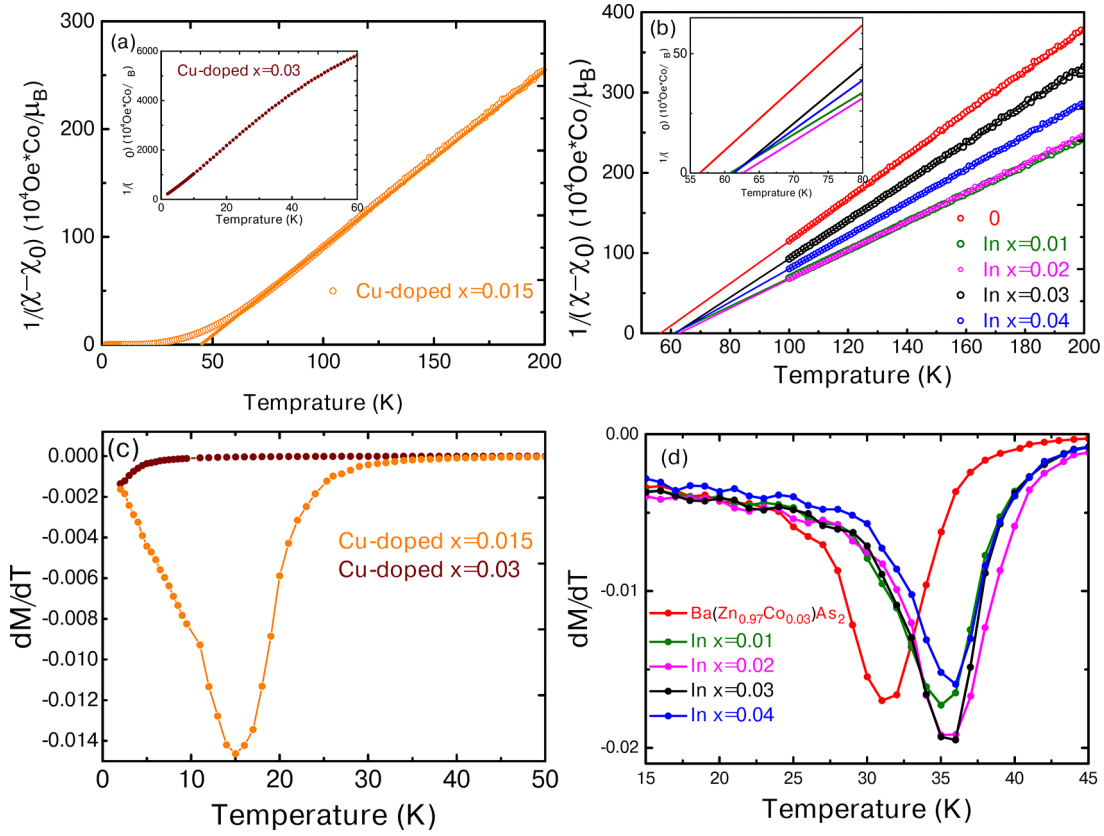

Fig. 4. (**a**, **b**) $(\chi - \chi_0)^{-1}$ versus temperature plots for Cu-doped and In-doped samples. Straight lines show the linear fitting, and the fitting temperature range is from 100 K to 200 K. (**c**, **d**) $dM(T)/dT$ versus temperature plots for Cu-doped and In-doped samples. T_C were determined as the temperature showing a minimum of these curves.

Doping level x	T_C (K)	θ (K)	μ_{eff} (μ_B/Co)	M_{2K} (μ_B/Co)
Cu-doped 0.03	0	− 1	1.7	0.004
Cu-doped 0.015	15	43	1.5	0.181
$Ba(Zn_{0.97}Co_{0.03})_2As_2$	31	56	1.4	0.210
In-doped 0.01	35	61	1.6	0.245
In-doped 0.02	36	63	1.6	0.267
In-doped 0.03	36	61	1.4	0.250
In-doped 0.04	36	61	1.4	0.211

Table 1. The Curie temperature T_C from the minimum value of $dM(T)/dT$, the Weiss temperature θ, the effective moment μ_{eff} from Curie–Weiss fit and the base magnetization M_{2K} measured at 2 K under FC mode for different doping levels x.

Experimental characterization

The X-ray diffraction (XRD) measurements were carried out on a PANalytical powder X-ray diffractometer with monochromatic Cu-$K_{\alpha 1}$ radiation. The DC magnetization measurements were conducted on a Quantum Design Magnetic Property Measurement System (MPMS-3). The Hall effect was measured on a Quantum Design Physical Property Measurement System (PPMS). The electrical resistivity was measured using the typical four-probe technique.

Data availability

All data generated or analysed during this study are included in this published article or available from the corresponding author on reasonable request.

Received: 20 December 2024; Accepted: 18 March 2025

Published online: 28 March 2025

References

1. Žutić, I., Fabian, J. & Sarma, S. Spintronics: Fundamentals and applications. *Rev. Mod. Phys.* **76**, 323–410 (2004).
2. Dietl, T. & Ohno, H. Dilute ferromagnetic semiconductors: Physics and spintronic structures. *Rev. Mod. Phys.* **86**, 187–251 (2014).
3. Dietl, T. et al. Spinodal nanodecomposition in semiconductors doped with transition metals. *Rev. Mod. Phys.* **87**, 1311 (2015).
4. Tanaka, M. Recent progress in ferromagnetic semiconductors and spintronics devices. *Jpn. J. Appl. Phys.* **60**, 010101 (2020).
5. Guo, S. & Ning, F. Progress of novel diluted ferromagnetic semiconductors with decoupled spin and charge doping: Counterparts of Fe-based superconductors. *Chin. Phys. B* **27**, 097502 (2018).
6. Gu, Y., Guo, S. & Ning, F. Progress on microscopic properties of diluted magnetic semiconductors by NMR and μSR. *J. Semicond.* **40**, 081506 (2019).
7. Takanashi, K. Creation and control of spin current in solids. *Jpn. J. Appl. Phys.* **49**, 110001 (2010).
8. Dietl, T. A ten-year perspective on dilute magnetic semiconductors and oxides. *Nat. Mater.* **9**, 965–974 (2010).
9. Ohno, H. et al. (Ga, Mn)As: A new diluted magnetic semiconductor based on GaAs. *Appl. Phys. Lett.* **69**, 363–365 (1996).
10. Sawicki, M. et al. Experimental probing of the interplay between ferromagnetism and localization in (Ga, Mn)As. *Nat. Phys.* **6**, 22–25 (2010).
11. Dietl, T., Ohno, H., Matsukura, F., Cibert, J. & Ferrand, D. Zener model description of ferromagnetism in zinc-blende magnetic semiconductors. *Science* **287**, 1019–1022 (2000).
12. Dietl, T., Ohno, H. & Matsukura, F. Hole-mediated ferromagnetism in tetrahedrally coordinated semiconductors. *Phys. Rev. B* **63**, 195205 (2001).
13. Chen, L. et al. Enhancing the Curie temperature of ferromagnetic semiconductor (Ga, Mn)As to 200 K via nanostructure engineering. *Nano. Lett.* **11**, 2584–2589 (2011).
14. Hai, P. N. et al. Growth and characterization of n-type electron-induced ferromagnetic semiconductor (In, Fe)As. *Appl. Phys. Lett.* **101**, 182403 (2012).
15. Deng, Z. et al. Li(Zn, Mn)As as a new generation ferromagnet based on a I–II–V semiconductor. *Nat. Commun.* **2**, 1–5 (2011).
16. Deng, Z. et al. Diluted ferromagnetic semiconductor Li(Zn, Mn)P with decoupled charge and spin doping. *Phys. Rev. B* **88**, 081203 (2013).
17. Ding, C. et al. $(La_{1-x}Ba_x)(Zn_{1-x}Mn_x)AsO$: A two-dimensional 1111-type diluted magnetic semiconductor in bulk form. *Phys. Rev. B* **88**, 041102 (2013).
18. Zhao, K. et al. New diluted ferromagnetic semiconductor with Curie temperature up to 180 K and isostructural to the '122' iron-based superconductors. *Nat. Commun.* **4**, 1–5 (2013).
19. Zhao, K. et al. Ferromagnetism at 230 K in $(Ba_{0.7}K_{0.3})(Zn_{0.85}Mn_{0.15})_2As_2$ diluted magnetic semiconductor. *Chin. Sci. Bull.* **59**, 2524–2527 (2014).
20. Chen, B. et al. New fluoride-arsenide diluted magnetic semiconductor (Ba, K)F(Zn, Mn) As with independent spin and charge doping. *Sci. Rep.* **6**, 1–9 (2016).
21. Yang, X. et al. K and Mn co-doped $BaCd_2As_2$: A hexagonal structured bulk diluted magnetic semiconductor with large magnetoresistance. *J. Appl. Phys.* **114**, 223905 (2013).
22. Ning, F. et al. Suppression of T_C by overdoped Li in the diluted ferromagnetic semiconductor $Li_{1+y}(Zn_{1-x}Mn_x)P$: A μSR investigation. *Phys. Rev. B* **90**, 085123 (2014).
23. Guo, S. et al. $Ba(Zn, Co)_2As_2$: A diluted ferromagnetic semiconductor with n-type carriers and isostructural to 122 iron-based superconductors. *Phys. Rev. B* **99**, 155201 (2019).
24. Fu, L. et al. Drastic improvement of Curie temperature by chemical pressure in N-type diluted magnetic semiconductor $Ba(Zn, Co)_2As_2$. *Sci. Rep.* **11**, 7652 (2021).
25. Zhi, G. et al. First-principles study on the electronic structure of n-type magnetic semiconductor $Ba(Zn_{1-x}Co_x)_2As_2$. *New J. Phys.* **26**, 033030 (2024).
26. Klüfers, P. & Mewis, A. Zur struktur der verbindungen $BaZn_2P_2$ und $BaZn_2As_2$/The crystal structure of $BaZn_2P_2$ and $BaZn_2As_2$. *Z. Naturforsch. B* **33**, 151–155 (1978).
27. Hellmann, A., Löhken, A., Wurth, A. & Mewis, A. Neue arsenide mit $ThCr_2Si_2$-oder einer damit verwandten struktur: Die verbindungen ARh_2As_2 (A: Eu, Sr, Ba) und $BaZn_2As_2$/New arsenides with $ThCr_2Si_2$-type or related structures: The compounds ARh_2As_2 (A: Eu, Sr, Ba) and $BaZn_2As_2$. *Z. Naturforsch. B* **62**, 155–161 (2007).
28. Xiao, Z. et al. Epitaxial growth and electronic structure of a layered zinc pnictide semiconductor, β-$BaZn_2As_2$. *Thin Solid Films* **559**, 100–104 (2014).
29. Toby, B. & Von Dreele, R. B. GSAS-II: the genesis of a modern open-source all purpose crystallography software package. *J. Appl. Crystallogr.* **46**, 544–549 (2013).
30. Ren, Q. et al. Establishing the carrier scattering phase diagram for zrnisn-based half-heusler thermoelectric materials. *Nat. Commun.* **11**, 3142 (2020).
31. Han, W. et al. Li(Cd, Mn)P: A new cadmium based diluted ferromagnetic semiconductor with independent spin & charge doping. *Sci. Rep.* **9**, 7490 (2019).
32. Xiao, Z. et al. Narrow bandgap in β-$BaZn_2As_2$ and its chemical origins. *J. Am. Chem. Soc.* **136**, 14959–14965 (2014).

Acknowledgements

The work at Zhejiang was supported by National Key R&D Program of China (No. 2022YFA1403202, 2022YFA1402701), NSF of China (No. 12074333), the Key R&D Program of Zhejiang Province, China (2021C01002).

Author contributions

F.L.N., L.C.F. and X.Q.Z conceived this work, X.Q.Z. and L.C.F. conducted the experiments with the help of J.O.D., L.F.X., X.P., H.Y.T. and Z.C.X, results were analysed by X.Q.Z., L.C.F., Q.L.Y., G.X.Z. and Y.L.G., all authors contributed to the preparation of this manuscript.

Declarations

Competing interests

The authors declare no competing interests.

Additional information

Correspondence and requests for materials should be addressed to L.F. or F.N.